International Journal for Housing Science and Its Applications
Publish August 10, 2025. Volume 46, Issue 4 Pages 715-725

https://doi.org/10.70517/ijhsa46465

# Construction of real-time monitoring and regulation system of distributed photovoltaic in virtual power plant based on edge computing technology

**Junyu Liang[1,*], Xiaosong Zeng[2], Yiran Rao[3], Xuehao He[1] and Xiaoguo Xiong[3]**
[1] Electric Power Institute, Yunnan Power Grid Company Ltd, Kunming, Yunnan, 650217, China
[2] Yunnan Power Grid Energy Investment Co., Ltd, Kunming, Yunnan, 650217, China
[3] Shenzhen KZCloud Technology LLC., Shenzhen, Guangdong, 518000, China
Corresponding authors: (e-mail: p_ELECT@163.com).

**Abstract** Under the background of the current energy structure transformation, the proportion of distributed photovoltaic power generation in the power system is increasing, but its intermittency and uncertainty bring serious challenges to the stable operation of the power grid. In this paper, for the traditional virtual power plant in distributed PV monitoring and regulation of the lack of real-time and data processing delay problems, constructed a virtual power plant based on edge computing technology distributed PV real-time monitoring and regulation system. The study adopts centralized and decentralized control mode, taking edge computing nodes as the low-level control and the virtual power plant energy management center as the high-level control. Five main influencing factors, namely, solar irradiance, ambient temperature, air humidity, wind speed and barometric pressure, are screened out by the gray correlation method, and an improved LSTM-TCN prediction model is constructed for the ultra-short-term output prediction of distributed photovoltaic. Based on the experimental data validation at five sites in Australia, the LSTM-TCN model has an MAE of 0.0388 and an RMSE of 0.0759 in typical summer scenarios, which improves the accuracy by 2.59% and 6.21%, respectively, compared with the traditional LSTM model. In the IEEE 33-node distribution network example, the total system load is 12MW and the total installed capacity of PV is 9.0MW, the proposed method realizes the ideal characteristics of virtual power plant with strong internal coupling and weak external coupling. The results show that the virtual power plant architecture based on edge computing can significantly improve the prediction accuracy of distributed PV and the system regulation effect, which provides an effective technical solution for building a smart grid.

**Index Terms** Edge computing, virtual power plant, distributed PV, LSTM-TCN, real-time monitoring, regulation system

## I. Introduction

In recent years, driven by the active promotion of national policies and technological innovation, distributed photovoltaic power generation technology has made significant progress, installed capacity continues to climb, and the pattern of photovoltaic development is gradually shifting from centralized to centralized and distributed [1]-[3]. However, the output of distributed PV is affected by a variety of factors such as weather, light intensity, etc., with significant randomness and volatility, and its regulation mode has the risk of communication, computation, and control failure, and distributed energy represented by distributed photovoltaic is difficult to be connected to the grid independently due to the limitation of its own characteristics, which has brought a great challenge to the safe and stable operation of the power system [4]-[7]. The proposal of virtual power plant provides new ideas to solve these problems.

Virtual power plant aggregates different types of distributed energy resources such as distributed energy sources, energy storage systems, controllable loads, electric vehicles, etc. through advanced control, metering, communication and other technologies, and realizes the coordinated and optimized operation of multiple distributed energy sources through a higher level of software architecture, which is more conducive to rational and optimal allocation and utilization of resources [8]-[10]. For example, when the user's power is in surplus, the corresponding regulation system will automatically transmit and distribute the excess power to other regions, and when the user's power is insufficient, it can be supplemented in time to ensure the balance and stability of the entire power supply system. The virtual power plant emphasizes more on the functions and effects presented to the outside world, updating the operation concept and generating social and economic benefits, and its basic application scenario is the power market [11], [12]. However, the decision-dependent uncertainty of distributed PV brings additional

challenges to virtual power plant scheduling [13]. And the existing virtual power plant itself suffers from defects such as data silos, missing sudden change data, and insufficient edge data processing [14], [15]. In this context, it is of great theoretical and practical significance to construct a real-time monitoring and regulation system for distributed photovoltaics in virtual power plants.

In the process of global energy transition, renewable energy, especially distributed photovoltaic (PV) power generation technology is developing rapidly, and has become an important part of the modern power system. Distributed photovoltaic power generation has the advantages of being clean and environmentally friendly, nearby consumption, and reducing transmission losses, but its inherent intermittency, volatility, and uncertainty characteristics pose new challenges to the safe and stable operation of the power grid. The traditional centralized power system is difficult to effectively coordinate and manage a large number of decentralized photovoltaic power generation units, and there is an urgent need to establish a new type of energy management and regulation system. As an innovative energy aggregation management model, virtual power plant, through information and communication technology, will be distributed power generation units, energy storage equipment and controllable loads and other resources for unified coordination and control, to improve the utilization rate of renewable energy, enhance the flexibility of the grid, optimize the participation of the power market and so on, showing great potential. However, the existing virtual power plant system faces technical bottlenecks such as data transmission delay, centralized computational load, and difficulty in real-time guarantee when dealing with massive distributed PV data, which limits its effectiveness in large-scale applications. The rise of edge computing technology provides a new solution idea to solve these problems, and by deploying nodes with computing, storage, and network functions at the edge of the network, the data can be processed in close proximity to reduce the network transmission overhead and improve the system response speed.

Based on the above problems and technology development trend, this study proposes a virtual power plant distributed photovoltaic real-time monitoring and control system construction program based on edge computing technology. Firstly, we design the virtual power plant architecture based on edge computing, adopt the control mode combining centralized and decentralized, and realize data processing and pre-analysis in the vicinity by deploying edge computing nodes. Then the gray correlation analysis method is used to identify the key meteorological factors affecting the PV power, and an improved LSTM-TCN deep learning prediction model is constructed to improve the PV power prediction accuracy. Finally, a virtual power plant and distribution network co-dispatch optimization model is established to verify the effectiveness and practicality of the proposed method through examples, providing technical support for the efficient utilization of distributed PV resources and the intelligent development of power systems.

## II. Real-time monitoring system for distributed photovoltaic based on edge computing technology

### *II. A. Virtual power plant based on edge computing*

#### II. A. 1) **Edge computing based virtual power plant architecture design**

In order to solve the realistic problems such as insufficient real-time in the existing virtual power plant, this paper proposes an edge computing-based virtual power plant architecture, which mainly includes several parts of distributed renewable energy units, customer loads, controllable generator sets, distributed energy storage devices, and control coordination center.

Edge computing-based virtual power plant [16] architecture adds edge computing nodes in the information communication path between each distributed energy source, customer load, distributed energy storage and distributed fuel units and the virtual power plant coordination and control center, collects smart meter data and processes the transmitted power generation and consumption data to shorten the latency and reduce the computing pressure on servers in the control and coordination center.

In terms of logical applications, edge computing nodes (ECNs) can be divided into four categories, namely intelligent devices, lightweight computing systems, intelligent gateway systems and intelligent distributed systems. They all have the characteristics of digitalization, networking, and intelligence, and they are able to provide resource technologies such as network, computing, and storage. The edge computing-based virtual power plant architecture designed in this paper adopts a centralized and decentralized control model, with the edge computing nodes as the low-level control and the virtual power plant energy management center as the high-level control. The optimized operation of the virtual power plant is jointly completed by the edge computing module and the energy management center, the edge computing nodes collect data and do pre-processing, and the energy management center receives the processing results for computing and generating the optimal decision scheme.

II. A. 2) **Smart Terminal Design in Edge Computing Nodes**

The coordinated control of the virtual power plant cannot be separated from the perfect metering technology, which can help the virtual power plant to grasp the operation information status of different units within the virtual power plant, and control the output conditions of the distributed power supply of the virtual power plant. Intelligent metering technology through the initiative of intelligent monitoring terminals, collect power generation and electricity data and obtain the user's cold, hot, electrical and water and other energy consumption demand and energy supply, to realize self-service meter reading, to determine the energy demand and supply in the region to provide important technical support. To realize the intelligent operation of the virtual power plant, it is necessary to rely on smart metering technology to realize the balance of energy management within the distributed energy, user loads, etc., so that it can not only obtain the energy demand within the virtual power plant in real time, but also make decisions on the energy supply in time, so as to achieve the goal of balancing the supply and demand of energy.

The overall system module design of the smart terminal is mainly divided into 3 parts: the core part is the master control unit, the controlled unit and the serial communication and human-computer interaction module. To carry out remote control and data collection and monitoring through the algorithms built into the smart metering equipment or with the commands and algorithms in the cloud backend management system, it is necessary to realize the design of real-time communication functions between the smart metering equipment and the cloud backend management system, and the smart terminal uploads the collected distributed energy outputs and user-side loads to the server side of the edge computing node through Ethernet, WIFI and so on.

## *II. B. **Distributed PV power prediction model construction***

### II. B. 1) Obtaining Predictive Model Training Data

There are many influencing factors that can cause the PV power value to produce changes, so it is necessary to select and exclude some minor influencing factors, so as to improve the efficiency of the operation. Gray correlation method selection, the specific process is as follows:

Step 1: List all the factors that can have an impact on the role of the factors as candidate factors.

Step 2: Compose the candidate factors into a comparison sequence $a_i^p$ with the following expression:

$$\left\{a_i^p \mid p=1,2,\cdots,m\right\} \tag{1}$$

Step 3: Establish a reference sequence of candidate factors $b^p$, which is generally composed of comparative ideal values and is composed in the following form:

$$\left\{b^p \mid p=1,2,\cdots,m\right\} \tag{2}$$

Step 4: The types of candidate factors are diverse, which inevitably results in different magnitudes, so in order to facilitate the comparison of each candidate factor in the two sequences constructed above, it is necessary to dimensionless $a_i^p$ with the following expression:

$$c_i^p = \frac{a_i^p - \frac{\sum_{p=1}^{m} a_i^p}{m}}{\varepsilon} \tag{3}$$

where $\varepsilon$ represents the variance.

Step 5: Calculate the absolute difference $A_i^p$ of the candidate factors in the two sequences with the following formula:

$$A_i^p = \left|b^p - c_i^p\right| \tag{4}$$

Select the maximum difference and minimum difference from all $A_i^p$ calculated, which are denoted as $\max A_i^p$, $\min A_i^p$, respectively.

Step 6: Calculate the correlation coefficient $B_i^p$ based on $\max A_i^p$, $\min A_i^p$ with the following formula:

$$B_i^p = \frac{\min A_i^p + c\max A_i^p}{A_i^p + \max A_i^p} \tag{5}$$

where $c$ represents the resolution coefficient, which takes the value in the range of $0 < c < 1$.

Step 7: Calculate the correlation degree. The formula is as follows:

$$C_i = \frac{\sum_{p=1}^{m} B_i^p}{m} \tag{6}$$

where $C_i$ is the correlation of the $i$ th candidate factor.

Step 8: Sort $C_i$ in descending order and select the top $k$ indicators as the main influencing factors that cause changes in PV power values.

After the above eight steps, a total of five indicators were selected, namely, solar irradiance, ambient temperature, air humidity, wind speed, and barometric pressure. The selected influencing factors are meteorological factors, and the differences in meteorology directly affect the PV power values, so only data with similar meteorological dates can guarantee the accuracy of the prediction.

Similar dates are selected by the following similarity formula:

$$D(r_j, r_k) = \frac{\sum_{i=1}^{5} r_{ji} r_{ki} - \frac{\sum_{i=1}^{5} r_{ji} \sum_{i=1}^{5} r_{ki}}{5}}{\sqrt{\left(\sum_{i=1}^{5} r_{ji}^2 - \frac{\left(\sum_{i=1}^{5} r_{ji}\right)^2}{5}\right)\left(\sum_{i=1}^{5} r_{ki}^2 - \frac{\left(\sum_{i=1}^{5} r_{ki}\right)^2}{5}\right)}} \tag{7}$$

where $D(r_j, r_k)$ represents the similarity between the $j$ th day and the $k$ th day; $r_{ji}$ represents the $i$ th influencing factor on the $j$ th day; and $r_{ki}$ represents the $i$ th influencing factor on the $k$ th day. Dates with $D(r_j, r_k)$ greater than 1.0 are selected, and the influencing factors as well as the PV power data are collected for these dates, which are composed into a complete training sample for the prediction model.

**II. B. 2) Improved LSTM-TCN Prediction Models**

LSTM [17] is known as Long Short-Term Memory Neural Network and TCN is known as Temporal Convolutional Network, in order to improve the accuracy of the prediction model, the two are combined to construct the prediction model, and the improved LSTM-TCN prediction model is trained. The specific process is as follows:

Step 1: Input 5 influence factors of distributed PV power from $N$ samples and normalize them.

Step 2: The influencing factors enter the first TCN layer, and sub-convolution, i.e., causal convolution and inflation convolution, is performed on the influencing factors. The convolution formulas are as follows, respectively:

Causal convolution:

$$(F \cdot R)(q) = \sum_{x=1}^{S} f_x r_{q-S+x} \tag{8}$$

Expansion Convolution:

$$(F *_h \cdot R)(q) = \sum_{x=1}^{S} f_x r_{q-(S-x)h} \tag{9}$$

where $R$ represents the input sequence of influencing factors, $R = \{r_1, r_2, \cdots, r_S\}$; $F$ represents the set of filters; * denotes the convolution operation; $f_s$ represents the $s$ th convolution kernel; $S$ represents the size of the convolution kernel; $q$ represents the sequence element ordinal number; $h$ represents the expansion factor.

Step 3: The result after two convolutions of the TCN layer is taken as input to the second LSTM layer.The second LSTM layer needs to go through three gate operations as follows:

Oblivion gate:

$$f_t = \xi[v_f(J_{t-1}, I_t) + \lambda_f] \tag{10}$$

Input Gate:

$$i_t = \xi[v_i(J_{t-1}, I_t) + \lambda_i] \tag{11}$$

Output Gate:

$$o_t = \xi[v_o(J_{t-1}, I_t) + \lambda_o] \tag{12}$$

where $\xi$ represents the sigmoid activation function; $v_f$, $v_i$, and $v_o$ represent the weight matrices of the three gates, respectively; $J_{t-1}$ represents the short-term state of the output at moment $t-1$;The $I_t$ represents the network input variable at moment $t$, which is the output of the TCN layer; The $\lambda_f$, $\lambda_i$, and $\lambda_o$ represent the bias terms of the three gates, respectively.

Step 4: After the operations of the three gate cells, the storage cell updates its own state, transforming from $l_{t-1}$ to $l_t$.

Step 5: Output the prediction result with the following equation:

$$Y_t = o_t \times \tanh l_t \tag{13}$$

where $Y_t$ represents the output prediction result.

Step 6: Judge whether the difference between $Y_t$ and the expected PV power of the training sample is less than or equal to the set threshold. If it is less than, the best trained prediction model is retained; otherwise, reverse error propagation is performed until the above threshold is satisfied.

### *II. C. Ultra-short-term output prediction of distributed PV based on LSTM-TCN*

The experimental data were collected from a distributed photovoltaic installation in Australia. The installation consists of five sites, with installed capacities of 1050.25, 23.4, 39.7, 46.6, and 108.2 kW at sites 1-5, respectively.The available meteorological characterization data include: temperature, horizontal total radiation, and daily rainfall, totaling three items. Meteorological data and output data are collected at a frequency of 10 minutes, and the characteristic data of the previous 10 time nodes predict the output data of the next time node, which is an ultra-short-term prediction. This experiment utilizes meteorological data and outflow data from 2021 to 2022, with 2021 data as the training set and 2022 data as the test set. Taking site 1 as an example, the average daily output and trend terms of site 1 are shown in Fig. 1. The results show that in the overall trend of the model, the mean value of the average daily outflow of site 1 is around 0.1792 and all the values of the average daily outflow are below 0.3. The overall fluctuation of the trend term of the model is small and shows a trend of increasing, then less, then increasing.

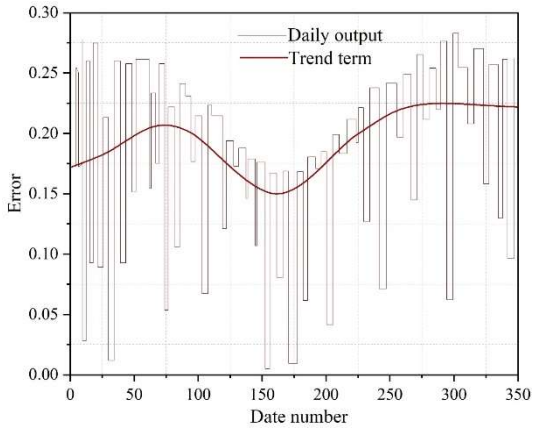


Figure 1: Daily output and trend items of site 1

The trend term for site 1 was obtained by 160 times moving average, Figure 2 demonstrates the results of different times of moving average, it can be seen that there is a good smoothness of data after 160 times moving average. The neighborhood matrix of the correlation diagram constructed from the Pearson correlation coefficient of the output data of each site. It can be seen that sites 2, 4, and 5 are extremely strongly correlated with each other, sites 3 and 4 are strongly correlated with each other, and site 1 is weakly correlated with other sites.

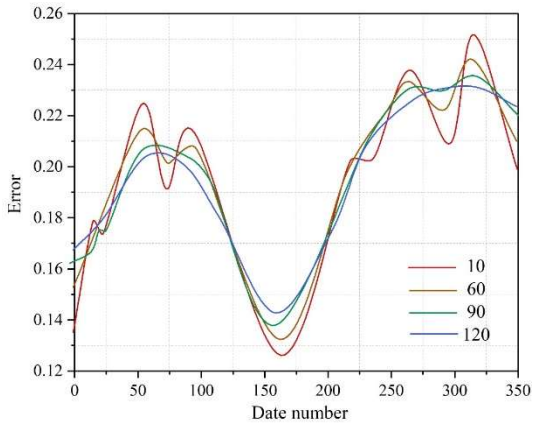


Figure 2: The average result of different times

The number of layers of the LSTM-TCN prediction network is set to 4, the time step is set to 12, and the dropout rate is set to 0.01. The traditional LSTM network is used as a comparison with the same parameter settings as LSTM-TCN. The prediction results for the first prediction day of site 1 are shown in Fig. 3. It can be seen that between days 0-45, both models are very close to the true value. Between days 45-120 and 140-190, the model of this paper is even closer to the true value.

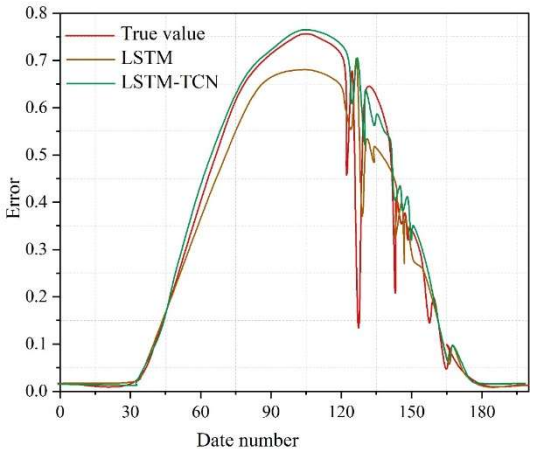


Figure 3: The prediction of the first forecast day of the site 1

It should be noted that, since the installed capacity of site 1 is much higher than the other four sites in this experiment, calculating the EMAE and ERMSE with the original data will make the weight of the error of site 1 too large, which is not conducive to the global measurement of the error of all sites, so the normalized data are chosen to calculate the EMAE and ERMSE. Three scenarios, namely, summer typical, winter typical, and year-round average, are used to evaluate the accuracy of the model. Taking site 1 as an example, the predicted results of typical summer days at site 1 are shown in Fig. 4; the predicted results of typical winter days at site 1 are shown in Fig. 5. It can be seen that before normalization, there is a significant error between 125-160 between the prediction results of the two models and the true value. This may be caused by the larger installed capacity at Site 1.

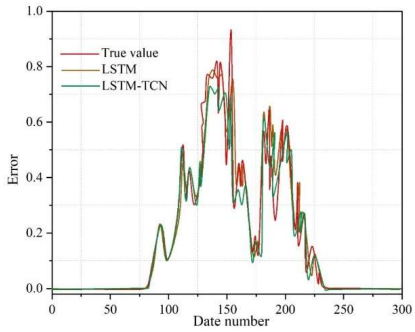


Figure 4: The site 1 summer typical day prediction results

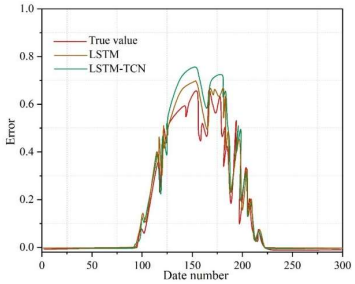


Figure 5: The site 1 winter typical day prediction results

In order to evaluate the model effect, the typical summer selects the full-month data of January, the typical winter selects the full-month data of July, and the average of the whole year selects the data of the first 10 days of each month, and the errors are calculated separately, and the errors of different sub-scenarios of the model and the results of the calculation of this progress are shown in Table 1. The calculation results show that the LSTM-TCN model is better than the LSTM model as a whole, and the prediction accuracy is significantly improved. It can be seen that the method of preprocessing with extracted trend terms is beneficial to both the LSTM-TCN model and the LSTM model to improve the accuracy. However, the annual average accuracy of LSTM without extracting the trend term is better than that of LSTM-TCN, which indicates that the method of extracting the trend term may have some limitations, and in practical applications, we can try both the methods of extracting and not extracting the trend term, and choose the optimal solution according to the test results.

Table 1: Error of different field view model and the results of this progress

| Error | Model and test indicators | Scene | | |
|---|---|---|---|---|
| | | Summer typical | Winter typical | Annual average |
| EMAE / ERMSE | LSTM-TCN | 0.0388/ 0.0759 | 0.0388/ 0.0897 | 0.0376/ 0.0835 |
| | LSTM | 0.0387/ 0.0819 | 0.0569/ 0.1012 | 0.0486/ 0.0951 |
| Error improvement | MAE (%) | 2.59 | 28.46 | 20.36 |
| | RMSE (%) | 6.21 | 11.03 | 12.62 |

## III. Application effect of distributed photovoltaic real-time monitoring and regulation system of virtual power plant

### *III. A. Co-scheduling model for virtual power plant and distribution network*

In the original distribution network structure, the distribution system contains only one flexibility resource, MT, which is dispatched to provide additional power when voltage overruns occur in the distribution system, at which time the generation cost is high. By introducing flexible resources with lower generation costs, such as distributed photovoltaic [18] and distributed energy storage, they can effectively participate in the operation of the distribution market, releasing their flexibility and reducing the generation costs, which ensures the economic efficiency of the distribution system.

#### III. A. 1) Objective function

The virtual power plant, as one of the distribution market participants, can be operated in conjunction with the distribution network, which at this point is aimed at minimizing the total cost, which includes the cost of the first node and the cost of the generation of various VPPs. This can be expressed as follows:

$$\min \sum_{t\in\Omega_T}\left[\sigma_t Pg_{1,t}+\pi^{PV}P_{j,t}^{PV}+\pi^{MT}P_{j,t}^{MT}+\pi^{BESS}P_{j,t}^{ES,C}/\eta-\eta P_{j,t}^{ES,D}\right] \tag{14}$$

where, $\sigma_t$ is the power purchase price of the substation node from the higher grid in time period $t$, $Pg_{1,t}$ is the power purchase of the substation node from the higher grid in time period $t$, and $\eta$ is the charging and discharging efficiency of the distributed energy storage. $P_{j,t}^{PV}$ / $P_{j,t}^{MT}$ and $\pi^{BESS}$ / $\pi^{PV}$ / $\pi^{MT}$ are the active power and the cost price of the distributed energy storage/distributed photovoltaic/diesel generator, respectively.

#### III. A. 2) Constraints

In this section, a safe operation model of the distribution network considering network losses is developed based on the branch-current model, which contains the constraints such as power balance equations, power limitation constraints on active and reactive power of generators, voltage drop constraints, voltage constraints, and second-order cone planning constraints.

(1) Power balance constraints

For ease of representation, the power balance equation is split into two parts, active power and reactive power, as shown in the following equation:

$$Pg_{1,t}=\sum_{k\in C_1}P_{1k,t},Qg_{1,t}=\sum_{k\in C_1}Q_{1k,t},\forall t\in\Omega_T \tag{15}$$

$$Pg_{j,t}-P_{j,t}^{D}=\sum_{k:j\to k}P_{jk,t}-\sum_{i:i\to j}P_{ij,t}-R_{ij}l_{ij,t} \tag{16}$$

$$\forall j\in\Omega_N,t\in\Omega_T$$

$$Qg_{j,t} - Q_{j,t}^{D} = \sum_{k:j\to k} Q_{jk,t} - \sum_{i:i\to j} Q_{ij,t} - X_{ij} l_{ij,t} \quad \forall j \in \Omega_N, t \in \Omega_T \tag{17}$$

$$Pg_{j,t} = P_{j,t}^{PV} + P_{j,t}^{BESS} + P_{j,t}^{MT}, \forall j \in \Omega_N, t \in \Omega_T \tag{18}$$

$$Qg_{j,t} = Q_{j,t}^{PV} + Q_{j,t}^{BESS} + Q_{j,t}^{MT}, \forall j \in \Omega_N, t \in \Omega_T \tag{19}$$

where $N$ is the set of all nodes except the first node, $C_1$ represents the set of all children of the first node, $i$ and $j$ represent the parent and child nodes of a branch respectively, and $k$ represents the set of all children of node $j$. Among them, $Pg_{1,t} / Qg_{1,t}$ is the active/reactive power of the first node, which is transmitted to the distribution network by the upstream node, $P_{1k,t} / Q_{1k,t}$ represents the active/reactive power of the branch where the first node is located, $Pg_{j,t} / Qg_{j,t}$ is the active/reactive power of the node other than the first node, $P_{j,t}^{D} / Q_{j,t}^{D}$ is the active/reactive load of node $j$, $P_{ij,t}$ and $Q_{ij,t}$ represent the active/reactive power of the branch $i$ to $j$, $R_{ij} / X_{ij}$ is the line resistance and reactance, and $l_{ij,t}$ is the square of the current. $P_{j,t}^{PV} / Q_{j,t}^{PV}$, $P_{j,t}^{BESS} / Q_{j,t}^{BESS}$ and $P_{j,t}^{MT} / Q_{j,t}^{MT}$ represent the active/reactive power of PV, ES and MT, respectively, and the virtual power plant provides active and reactive power such as $P_{j,t}^{PV} / Q_{j,t}^{PV}$ and $P_{j,t}^{BESS} / Q_{j,t}^{BESS}$ works in tandem with the distribution network to reduce the net load of the distribution network nodes to alleviate the voltage out-of-limit problem.

(2) Constraints on the power limit of the first node:

$$P_{\min} \le Pg_{1,t} \le P_{\max}, \forall t \in \Omega_T \tag{20}$$

$$Q_{\min} \le Qg_{1,t} \le Q_{\max}, \forall t \in \Omega_T \tag{21}$$

where, $Pg_{1,t} / Qg_{1,t}$ is the active/reactive power of the first node, and $P_{\min} / P_{\max}$ and $Q_{\min} / Q_{\max}$ are the minimum/maximum values of the active/reactive power of the first node, respectively.

(3) Voltage Drop Constraints

According to Ohm's law, the voltage drop constraint of a line is expressed as:

$$V_{i,t} - V_{j,t} = Z_{ij} I_{ij,t} \tag{22}$$

where $V_{i,t} / V_{j,t}$ is the branch parent/child node voltage, $I_{ij,t}$ is the branch $ij$ current, and $Z_{ij} = R_{ij} + jX_{ij}$ is the line impedance. Multiplying their conjugate complexes on both the left and right sides of the equation above while defining $v_{i,t} = V_{i,t} V_{i,t}^{*}$ and $v_{j,t} = V_{j,t} V_{j,t}^{*}$, the above equation can be further rewritten as:

$$v_{j,t} = v_{i,t} - 2R_{ij} P_{ij,t} + X_{ij} Q_{ij,t} + R_{ij}^{2} + X_{ij}^{2} l_{ij,t} \tag{23}$$

(4) Voltage limitation constraints:

$$v_{1,t} = V_{1,t}^{ref\,2}, t \in \Omega_T \tag{24}$$

$$V_{j,t}^{\min 2} \le v_{j,t} \le V_{j,t}^{\max 2}, \forall j \in \Omega_N, t \in \Omega_T \tag{25}$$

The above equation restricts the voltage range of all nodes, where $v_{1,t}$ is the first node voltage, $V_{1,t}^{ref}$ is the reference voltage, and $V_{j,t}^{\min}$ and $V_{j,t}^{\max}$ represent the upper and lower bounds of the voltage limitation constraints, which are set to 0.99 and 1.01 p.u., respectively.

(5) Second-order cone planning constraint

The branch first end power can be expressed in the following mathematical form:

$$S_{ij,t} = V_{i,t} I_{ij,t}^{*} \tag{26}$$

where $S_{ij,t}$ is the branch complex power and $S_{ij,t} = P_{ij,t} + jQ_{ij,t}$. Defining $l_{ij,t} = I_{ij,t} I_{ij,t}^{*}$, the above equation can be reduced to:

$$l_{ij,t} = \frac{P_{ij,t}^{2} + Q_{ij,t}^{2}}{v_{i,t}} \tag{27}$$

The above equation contains a quadratic equation, which leads to a non-convex model, which is rewritten as a rotated second-order conic plan for ease of solution and relaxation of the feasible domain, as shown below:

$$\left\| \begin{matrix} 2P_{ij,t} \\ 2Q_{ij,t} \\ l_{ij,t} - v_{i,t} \end{matrix} \right\|_2 \le l_{ij,t} + v_{i,t} \tag{28}$$

where $\|x\|_2$ denotes the second paradigm of $x$.

(6) Diesel generator constraints:

$$0 \le P_{j,t}^{MT} \le P_{j,t}^{MT,\max} \tag{29}$$

$$0 \le Q_{j,t}^{MT} \le P_{j,t}^{MT} \tan \arccos \alpha_j \tag{30}$$

where, the constraint equations (29) and (30) limit the range of active and reactive output of the diesel generator. $P_{j,t}^{\mathrm{MT}} / Q_{j,t}^{\mathrm{MT}}$ is the active/reactive power of the MT, and $P_{j,t}^{MT,\max}$ is the maximal value of active power emitted by the MT.

### *III. B. Example analysis*

In this paper, a distribution network with a large number of PV and energy storage devices connected in IEEE33 nodes is used for example analysis. The total system load is 12 MW, the total installed capacity of PV is 9.0 MW, the total installed capacity of energy storage is 1.8 MW, and the voltage fluctuation range is ±2%. The modeling solution is carried out using Yalmip+Cplex.

#### III. B. 1) **Comparison with static division methods**

At the moment of 12:00, the static partitioning method is used to partition the active distribution network into optical storage virtual power plants, and the obtained inter-plant lines are 2, 8, and 26.The minimum supply rate and inter-plant power flow are shown in Fig. 6,where (a) and (b) represent the minimum supply rate and inter-plant flow power of the optical storage virtual power plants, respectively. The static partitioning results show that the system is partitioned into four optical storage virtual power plants with the maximum control dimension of 12 and the minimum of 3, indicating that the static partitioning can well reduce the control dimension of the power plants. However, the power plant obtained from static partitioning does not have a minimum power supply rate of 0.2 in 64% of the time of 1 d. At this time, it needs to be supplied with power through the power grid, which results in a higher peak power flow on the line. In this paper, the method of power plants rely on optical storage equipment to carry out joint complementary to meet the power needs of the whole day within the power plant, and power plants between the line power flow is less, highlighting the strong coupling within the power plant outside the weak coupling characteristics, which is beneficial to the regulation of power plants.

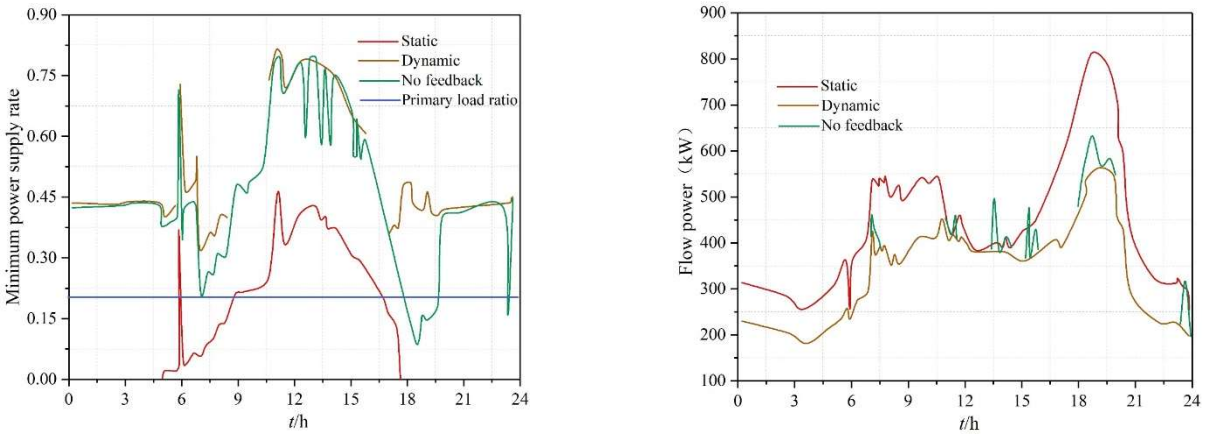


(a) Minimum power supply for virtual power plants (b) The flow power of the optical storage virtual factory

Figure 6: Minimum power rate and power flow between factories

#### III. B. 2) **Minimum supply rate and inter-plant power flow**

Steady state division and dynamic division without feedback are also carried out for this system, and the inter-plant lines obtained by steady state division are:2,7,10,15,12, and the minimum power supply rate of the block and the power flow between the blocks of the three methods are compared, and the minimum power supply rate and the inter-plant power flow are shown in Fig. 7, where (a) and (b) represent the minimum power supply rate of the virtual power plant of the optical storage and the inter-plant flow power, respectively. It can be seen that the power supply rate of the virtual power plant derived by the method of this paper is better, the value of inter-plant power flow is relatively minimal, and the division result has less variation and better division effect. The application of the actual power grid shows that the method of this paper has generality and practicability in the application of the actual

power grid. To sum up, the dynamic optimization division method of multiple time scales proposed in this paper is more superior and practical.

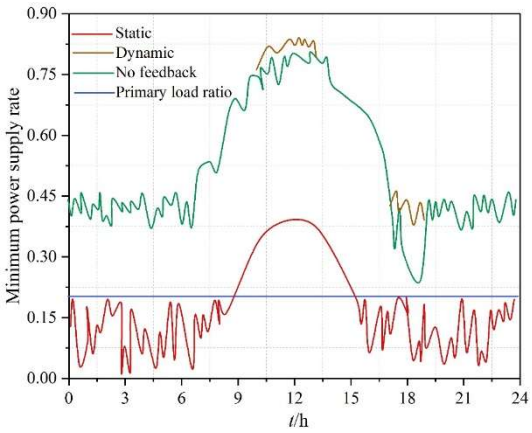


(a) Minimum power supply for virtual power plants

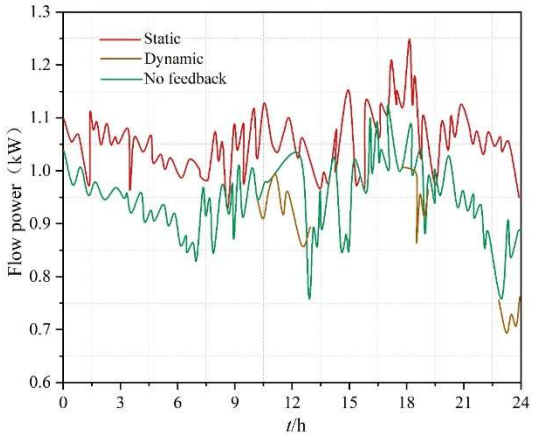


(b) The flow power of the optical storage virtual factory

Figure 7: Minimum power rate and power flow between factories

## IV. Conclusion

In this study, by constructing a real-time monitoring and regulation system for distributed PV in virtual power plants based on edge computing technology, the technical problems of traditional virtual power plants in real-time and data processing are effectively solved.

The introduction of edge computing nodes significantly shortens the data transmission delay, reduces the computing pressure of the control coordination center, and realizes the organic combination of centralized and decentralized control.

Gray correlation analysis successfully screens out five key influencing factors, namely, solar irradiance, ambient temperature, air humidity, wind speed and barometric pressure, which provides scientific input features for the PV power prediction model.

The improved LSTM-TCN prediction model performs well in the validation of five PV sites in Australia, with 28.46% and 11.03% improvement in MAE and RMSE metrics, respectively, compared with the traditional LSTM model in typical winter scenarios, which proves the prediction accuracy and stability of the model.

The analysis of the IEEE33 node distribution network example shows that under the system configuration of 9.0MW total installed capacity of PV and 1.8MW total installed capacity of energy storage, the proposed method realizes the ideal operation state of virtual power plant with strong internal coupling and weak external coupling, and the inter-plant power flow is significantly reduced, and the system operation efficiency is significantly improved.

The intelligent terminal under the edge computing architecture realizes real-time data interaction with the cloud backend through Ethernet, WIFI and other communication methods, which guarantees the reliability and practicability of the system.

This technical solution provides a feasible path for the intelligent management of large-scale distributed PV resources, and is of great significance for promoting the efficient utilization of energy and the construction of smart grid.

## Funding

This work was supported by Key Technology Research on Virtual Power Plant for Multi-Participant Cooperative Game in Distributed Energy under Yunnan Province Key Research and Development Program (202302AF080006) and Key Technology Research on Cooperative Operation of Virtual Power Plant for Multi-Participant Cooperative Game under Innovation Project of China Southern Power Grid Co., Ltd. (YNKJXM20240065).

## References

[1] Li, H., Lin, H., Tan, Q., Wu, P., Wang, C., De, G., & Huang, L. (2020). Research on the policy route of China's distributed photovoltaic power generation. Energy Reports, 6, 254-263.

[2] Li, K., Wang, F., Mi, Z., Fotuhi-Firuzabad, M., Duić, N., & Wang, T. (2019). Capacity and output power estimation approach of individual behind-the-meter distributed photovoltaic system for demand response baseline estimation. Applied energy, 253, 113595.

[3] Wang, Y., He, J., & Chen, W. (2021). Distributed solar photovoltaic development potential and a roadmap at the city level in China. Renewable and Sustainable Energy Reviews, 141, 110772.
[4] Li, Y., Wang, Y., & Chen, Q. (2020). Study on the impacts of meteorological factors on distributed photovoltaic accommodation considering dynamic line parameters. Applied energy, 259, 114133.
[5] Shang, B. O. (2019). Effects of Distributed Photovoltaic Power Generation on Stability of Electrical Voltage System. Nonlinear Optics, Quantum Optics: Concepts in Modern Optics, 50(4).
[6] Cheng, Z., Li, Z., Liang, J., Si, J., Dong, L., & Gao, J. (2020). Distributed coordination control strategy for multiple residential solar PV systems in distribution networks. International Journal of Electrical Power & Energy Systems, 117, 105660.
[7] Camilo, H. F., Udaeta, M. E. M., Gimenes, A. L. V., & Grimoni, J. A. B. (2017). Assessment of photovoltaic distributed generation–Issues of grid connected systems through the consumer side applied to a case study of Brazil. Renewable and Sustainable Energy Reviews, 71, 712-719.
[8] Lee, J., & Won, D. (2021). Optimal operation strategy of virtual power plant considering real-time dispatch uncertainty of distributed energy resource aggregation. IEEE Access, 9, 56965-56983.
[9] Wang, Y., Huang, W., Chen, H., Yu, Z., Hu, L., & Huang, Y. (2024). Optimal scheduling strategy for virtual power plants with aggregated user-side distributed energy storage and photovoltaics based on CVaR-distributionally robust optimization. Journal of Energy Storage, 86, 110770.
[10] Qiu, J., Meng, K., Zheng, Y., & Dong, Z. Y. (2017). Optimal scheduling of distributed energy resources as a virtual power plant in a transactive energy framework. IET Generation, Transmission & Distribution, 11(13), 3417-3427.
[11] Moreno, B., & Díaz, G. (2019). The impact of virtual power plant technology composition on wholesale electricity prices: A comparative study of some European Union electricity markets. Renewable and Sustainable Energy Reviews, 99, 100-108.
[12] Behi, B., Baniasadi, A., Arefi, A., Gorjy, A., Jennings, P., & Pivrikas, A. (2020). Cost–benefit analysis of a virtual power plant including solar PV, flow battery, heat pump, and demand management: A western australian case study. Energies, 13(10), 2614.
[13] Yu, J., Fan, Y., & Hou, J. (2025). Research on Distributed Optimization Scheduling and Its Boundaries in Virtual Power Plants. Electronics, 14(5), 932.
[14] Katiraei, F., Morovati, S., Chuangpishit, S., & Ghorashi, S. A. (2023). Virtual power plant empowerment in the next generation of data centers: Outlining the challenges. IEEE Electrification Magazine, 11(3), 35-44.
[15] Popławski, T., Dudzik, S., Szeląg, P., & Baran, J. (2021). A case study of a virtual power plant (VPP) as a data acquisition tool for PV energy forecasting. Energies, 14(19), 6200.
[16] Yuqiao Liu,Chen Pan,YeonJae Oh & Chang Gyoon Lim. (2025). Hybrid Memory-Enhanced Autoencoder with Adversarial Training for Anomaly Detection in Virtual Power Plants. Computers, Materials & Continua,82(3),4593-4629.
[17] Lijian Wei,Sihang Chen,Junqin Lin & Lei Shi. (2025). Enhancing return forecasting using LSTM with agent-based synthetic data. Decision Support Systems,193,114452-114452.
[18] Jiao Xing,Xiangqian Nie,Qimeng Li & Fan Xiao. (2025). Construction of distributed photovoltaic operation and maintenance knowledge base based on time series knowledge map. Discover Applied Sciences,7(5),409-409.